

The $O(n)$ loop model on a three-dimensional lattice

Qingquan Liu^a, Youjin Deng^{a,*}, Timothy M. Garoni^b, Henk W. J. Blöte^c

^aHefei National Laboratory for Physical Sciences at Microscale,

Department of Modern Physics, University of Science and Technology of China, Hefei, 230027, China

^bSchool of Mathematical Sciences, Monash University, Clayton, Victoria 3800, Australia

^cInstituut Lorentz, Leiden University, P.O. Box 9506, 2300 RA Leiden, The Netherlands

Abstract

We study a class of loop models, parameterized by a continuously varying loop fugacity n , on the *hydrogen-peroxide* lattice, which is a three-dimensional cubic lattice of coordination number 3. For integer $n > 0$, these loop models provide graphical representations for n -vector models on the same lattice, while for $n = 0$ they reduce to the self-avoiding walk problem. We use worm algorithms to perform Monte Carlo studies of the loop model for $n = 0, 0.5, 1, 1.5, 2, 3, 4, 5$ and 10 and obtain the critical points and a number of critical exponents, including the thermal exponent y_t , magnetic exponent y_h , and loop exponent y_l . For integer n , the estimated values of y_t and y_h are found to agree with existing estimates for the three-dimensional $O(n)$ universality class. The efficiency of the worm algorithms is reflected by the small value of the dynamic exponent z , determined from our analysis of the integrated autocorrelation times.

Keywords: Loop model; Monte Carlo; Worm algorithm;

PACS: 02.70.Tt, 05.10.Ln, 64.60.De, 64.60.F-

1. Introduction

Among the many model systems studied in the field of statistical mechanics, two fundamental examples that continue to play a central role are the n -vector model [1] and q -state Potts model [2, 3, 4]. Initially, the parameters n and q can assume only positive integer values. However, the Kasteleyn-Fortuin mapping [5] transforms the Potts model into the random-cluster model [6], in which q appears as a continuous parameter. Likewise, certain n -vector spin models on the honeycomb lattice can be mapped [7] to nonintersecting loop models which remain well-defined for non-integer n . Both types of mappings integrate out the original spin variables, while newly introduced bond variables define the remaining degrees of freedom. Each bond configuration can be represented by means of a graph covering a subset of the lattice edges. The transformed partition function specifies the statistical weight of each possible graph. This defines the probabilistic representation of the transformed model in terms of random geometric objects: clusters [5] and nonintersecting loops [7]. These geometric models play a major role in

*Corresponding author

Email addresses: liuqq@mail.ustc.edu.cn (Qingquan Liu), yjdeng@ustc.edu.cn (Youjin Deng), tim.garoni@monash.edu (Timothy M. Garoni), henk@lorentz.leidenuniv.nl (Henk W. J. Blöte)

recent developments of conformal field theory [8] via their connection with Schramm-Loewner evolution (SLE) [9, 10].

Given a particular lattice, or more generally a graph $G = (V, E)$, we consider the loop model defined for $n, x > 0$ by the partition function

$$Z = \sum_A n^{c(A)} x^{|A|}, \quad (1)$$

where the sum is over all configurations, A , of non-intersecting loops that can be drawn on the edges of G , $|A|$ denotes the number of occupied bonds, and $c(A)$ denotes the number of loops. It is well known [7] that on any graph of maximum degree 3, the model (1) arises for positive integer n as a loop representation of an n -component spin model,

$$Z = \text{Tr} \prod_{ij \in E} (1 + n x \mathbf{s}_i \cdot \mathbf{s}_j), \quad (2)$$

where the $\mathbf{s}_i = (s^1, \dots, s^n) \in \mathbb{R}^n$ are unit vectors and Tr denotes normalized integration with respect to any *a priori* measure $\langle \cdot \rangle_0$ on \mathbb{R}^n satisfying $\langle s^\alpha s^\beta \rangle_0 = \delta_{\alpha\beta}/n$ and $\langle s^\alpha \rangle_0 = \langle s^\alpha s^\beta s^\gamma \rangle_0 = 0$. In particular, uniform measure on the unit sphere is allowed, which results in an $O(n)$ symmetric spin model. In addition, various discrete *cubic* measures [7] are allowed, in which the spins are constrained to the unit hypercube; see Section 3.1. For each of these *a priori* measures, the model (2) with $n = 1$ is simply the Ising model.

For $n \neq 1$, the partition function (2) provides a high-temperature (small $\beta = xn$) approximation to the partition function of the n -vector model defined by the (reduced) Hamiltonian

$$\mathcal{H}(\mathbf{s}_1, \mathbf{s}_2, \dots) = -\beta \sum_{ij \in E} \mathbf{s}_i \cdot \mathbf{s}_j. \quad (3)$$

For spins on the unit sphere, the Hamiltonian (3) with $n = 2$ and $n = 3$, defines the standard XY and Heisenberg models, respectively, while its $n \rightarrow \infty$ limit corresponds to the spherical model [11, 1]. Since the partition function (2) shares the same symmetry as the Hamiltonian (3), one expects that for a given choice of spin *a priori* measure, the phase transitions of the two models will belong to the same universality class. We note that while (1) has a well-defined probabilistic meaning for all $n, x > 0$, the spin model (2) has positive weights only when $x < 1/n$. Finally, we recall [12] that the $n \rightarrow 0$ limit of the n -vector model corresponds to the self-avoiding walk (SAW) problem, however in this case the correspondence is not seen at the level of the partition function, but rather at the level of the two-point functions; see Sections 2.1 and 3.1.

On the honeycomb lattice, an exact analysis [13, 14, 15, 16] of the model (1) is possible, which yields the critical point and the universal exponents as a function of n in the range $-2 \leq n \leq 2$. For three-dimensional lattices, however, comparable exact results are not available, and approximations are necessary. These exist in the form of renormalization at a fixed number of dimensions [17], the ϵ -expansion [18], the $1/n$ expansion [19, 20, 21, 22], series expansions [1] and Monte Carlo simulations [23]. See [24] and references therein. In particular, Wolff's embedding algorithm [25] is a highly-efficient Monte Carlo method for studying the $O(n)$ spin model for integer $n > 0$.

Loop models with continuously varying n have recently been studied via Monte Carlo simulations [26, 27] in two dimensions, however, we are unaware of any similar studies in three dimensions. In [27], *worm* algorithms were presented for simulating the loop model (1) on any

3-regular graph¹ and for any real $n > 0$, and these algorithms were used to perform a systematic study of the loop model on the honeycomb lattice as a function of n . In the current article, we use the worm algorithms presented in [27] to perform an analogous study of the loop model on a three-dimensional 3-regular lattice, the so-called *hydrogen peroxide* lattice [28]. Since the hydrogen-peroxide lattice has coordination number 3, it provides a convenient setting for the study of high-temperature series [29, 30]. Therefore, given that worm algorithms simulate spaces of high-temperature graphs, it is also a natural setting for worm-algorithm studies in three dimensions.

For our purposes, the hydrogen-peroxide lattice is perhaps best understood as a subgraph of the simple-cubic lattice. The vertex set is \mathbb{Z}^3 , as for the simple-cubic lattice, however precisely half the edges are deleted from the neighborhood of each vertex, so that the edge set is $E_x \cup E_y \cup E_z$ where

$$\begin{aligned} E_x &= \{(x, y, z)(x + 1, y, z) : x, y, z \in \mathbb{Z}, z + x = 0 \pmod{2}\}, \\ E_y &= \{(x, y, z)(x, y + 1, z) : x, y, z \in \mathbb{Z}, x + y = 0 \pmod{2}\}, \\ E_z &= \{(x, y, z)(x, y, z + 1) : x, y, z \in \mathbb{Z}, y + z = 0 \pmod{2}\}. \end{aligned}$$

Since this lattice is a cubic (i.e. 3-regular) subgraph of the simple-cubic lattice, a more descriptive name may be the “cubic-cubic” lattice. Being both 3-regular and transitive, it is in some sense the natural three-dimensional analogue of the honeycomb lattice. The minimal cycles have length 10, with each vertex belonging to 10 such cycles and each edge to 15. A sketch of a finite patch wrapped on a 3-dimensional torus is shown in Fig. 1. Alternative drawings in which all angles are equal to 120° can be constructed [28] and are well-known in crystallography; the international number of such a lattice is 214 and its space group is $I4_132$. Both of these geometric configurations possess cubic symmetry.

We shall employ two variants of the worm algorithm in our simulations. The first version directly utilizes worm transitions that are in detailed balance with the appropriate loop weights $n^{c(A)} x^{|A|}$, and is valid for any $n \geq 0$. The $n \rightarrow 0$ limit of this version is equivalent to the Berretti-Sokal algorithm for SAWs. The second version combines the $n = 1$ worm algorithm with the coloring method [26, 27] to obtain an alternative algorithm which is valid for real $n \geq 1$. The advantage of second algorithm is that it avoids the need to perform non-local connectivity queries.

The details of these algorithms will be the subject of Section 2. Section 3 then describes the observables sampled in our simulations, which include a susceptibility-like quantity, and several dimensionless ratios. These are used to determine the critical points and the thermal and magnetic exponents by means of finite-size scaling. In addition, we present an estimator for the loop fractal dimension y_l . Finally, Section 4 presents the results of our simulations and our conclusions are summarized in Section 5.

2. Worm algorithms

Given a finite graph $G = (V, E)$, the cycle space, $C(G)$, is the set of all $A \subseteq E$ such that every site of G is incident to an even number of bonds in A . We call $A \subseteq E$ and (V, A) *Eulerian*

¹A k -regular graph has precisely k edges incident to each vertex. The descriptions “ k -regular” and “coordination number k ” are therefore synonymous.

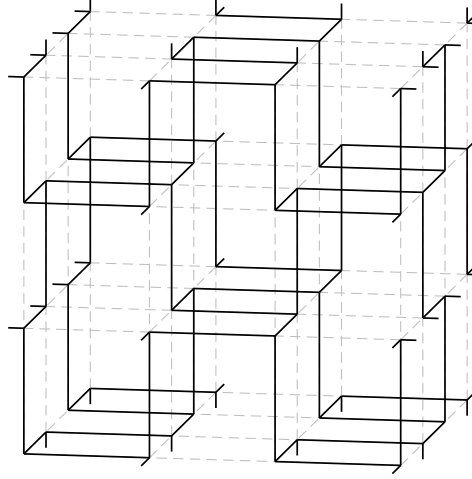


Figure 1: A 64-site hydrogen peroxide (cubic-cubic) lattice with periodic boundary conditions. The sites occupy the same positions as in a $4 \times 4 \times 4$ simple cubic lattice, however each site is adjacent to only 3 of the 6 edges allowed in the simple-cubic lattice.

whenever $A \in C(G)$. The worm algorithm provides a natural method for simulating loop models of the form

$$Z = \sum_{A \in C(G)} n^{c(A)} x^{|A|}, \quad (4)$$

where $c(A)$ is the cyclomatic number of the spanning subgraph (V, A) . The cyclomatic number of a graph is simply the minimum number of edges that need be deleted in order to make it cycle-free. Consequently, on graphs G of maximum degree 3 all Eulerian configurations $A \in C(G)$ consist of a collection of $c(A)$ nonintersecting loops, and the models (1) and (4) coincide in this case.

The essence of the worm idea is to enlarge the configuration space $C(G)$ to include two *defects* (i.e. vertices of odd degree), and to then move these defects via random walk. When the two defects happen to occupy the same site they *cancel*, and the resulting configuration becomes Eulerian once more. In the context of spin models, the state space of the worm dynamics corresponds to the space of high-temperature graphs of the two-point correlation function, as we describe in more detail in section 3.1. Worm algorithms for the high-temperature graphs of classical spin models were first formulated by Prokof'ev and Svistunov [31]. A careful investigation [32] of the dynamic behavior of the worm algorithm for the two- and three-dimensional Ising models showed that it suffers from only very weak critical slowing-down, especially in three dimensions where it was found that the Li-Sokal bound [33] appears to be very close to (or even exactly) sharp. In Section 4.5 we describe similar results for worm algorithms on the hydrogen peroxide lattice for $n = 2$. This contrasts markedly with the Swendsen-Wang algorithm, for which the Li-Sokal bound is far from sharp in three dimensions [34], and even more markedly with algorithms using simple local updates of the “plaquette” type [35], which have dynamic exponent $z > 2$. Furthermore, for certain observables, including the estimator for the

susceptibility, the worm algorithm was shown to display critical speeding-up [32]. A discussion of this estimator is the subject of Section 3.1.

In [27], the worm methodology was used to construct algorithms for the loop model (4) on any graph G for any real $n > 0$, and these algorithms were used to perform a systematic study of the loop model on the honeycomb lattice. In the current article, we apply the algorithms presented in [27] to the hydrogen peroxide lattice. In this section, we give a brief description of these algorithms; refer to [27] for more details, including a discussion of a version which remains provably ergodic as $x \rightarrow \infty$. Related worm algorithms, corresponding to the loop expansions of both (2) and (3), are presented in [36, 37].

2.1. Simple worm algorithm

It is most natural to describe the worm algorithm on an arbitrary finite graph $G = (V, E)$. For simplicity, we assume G is regular (i.e. each site has the same number of neighbours). For distinct vertices $u, v \in V$ we let $\mathcal{S}_{u,v}(G)$ denote the set of all subsets of E for which u and v are odd (i.e. have odd degree) with all other vertices being even, and we let $\mathcal{S}_{v,v}(G) = \mathcal{C}(G)$ for every $v \in V$. The state space of the worm algorithm is the set $\mathcal{S}(G)$ of all ordered triples (A, u, v) such that $u, v \in V$ and $A \in \mathcal{S}_{u,v}(G)$. We emphasize that in the context of spin models $\mathcal{S}_{u,v}(G)$ is nothing other than the set of high-temperature graphs of $\langle \mathbf{s}_u \cdot \mathbf{s}_v \rangle$, so that $\mathcal{S}(G)$ corresponds to the space of high-temperature graphs of the magnetization; see Section 3.1. The proposed moves of the worm algorithm are very simple: starting from $(A, u, v) \in \mathcal{S}(G)$ randomly choose one of the two defects; then randomly choose one of the neighbours of that defect; then move the chosen defect u to the chosen neighbour u' and flip the occupation status of the edge uu' , so that $A \rightarrow A \Delta uu'$. Here $A \Delta uu'$ denotes the symmetric difference of A with uu' : i.e. delete uu' if it is occupied, or add it if it is vacant. One then simply applies a standard Metropolis [38] acceptance/rejection prescription to determine the acceptance probabilities required to ensure the worm transitions are in detailed balance with the desired configuration weights $x^{|A|} n^{c(A)}$ on $\mathcal{S}(G)$. The resulting Monte Carlo algorithm is summarized in Algorithm 1. We emphasize that for any $(A, u, v) \in \mathcal{S}(G)$, if $u = v$ then $A \in \mathcal{C}(G)$, so by only measuring observables when $u = v$ one obtains a valid Markov-chain Monte Carlo method for the loop model.

Algorithm 1 (Simple worm algorithm).

loop

With probability p choose the first defect, otherwise choose the second

Uniformly at random, choose a neighbour u' of the chosen defect u

Propose the update $u \rightarrow u'$ and $A \rightarrow A \Delta uu'$, leaving the unchosen defect v fixed

Accept the proposed update with the acceptance probabilities given in Table 1

if $u' = v$ **then**

Sample observables

end if

end loop

The explicit acceptance probabilities used in our simulations are listed in Table 1. Rather than the typical choice of $\min(1, z)$ for the acceptance function we chose $z/(1+z)$, corresponding to a heat-bath algorithm [39]. We comment on this choice further below. We emphasize that, in general, the acceptance probabilities depend on the topology of the loops in a non-trivial way;

Table 1: Acceptance probabilities for the worm proposals $(A, u, v) \rightarrow (A \Delta uu', u', v)$. The same acceptance probabilities are used for the proposals $(A, v, u) \rightarrow (A \Delta uu', v, u')$.

$ A \Delta uu' - A $	$c(A \Delta uu') - c(A)$	$\mathbb{P}(A \Delta uu', u', v) / \mathbb{P}(A, u, v)$	Acceptance Probability
+1	+1	nx	$nx / (1 + nx)$
+1	0	x	$x / (1 + x)$
-1	-1	$1/(nx)$	$1 / (1 + nx)$
-1	0	$1/x$	$1 / (1 + x)$

we discuss this issue further below. The probability p in Algorithm 1 was set to $1/2$ in our simulations except when $n = 0$.

The $n \rightarrow 0$ limit of Algorithm 1 deserves some comment. By construction, the stationary distribution of the worm dynamics is

$$\pi_{G,n,x}(A, u, v) = \frac{n^{c(A)} x^{|A|}}{\sum_{(A', u', v') \in \mathcal{S}(G)} n^{c(A')} x^{|A'|}}. \quad (5)$$

As $n \rightarrow 0$, only those configurations with $c(A) = 0$ will retain positive weight, and therefore the support of $\pi_{G,n,x}(\cdot)$ in this limit reduces to the set of all paths (i.e. unrooted SAWs) on G . Likewise, the $n \rightarrow 0$ limit of Algorithm 1 provides a valid Monte Carlo algorithm for simulating this reduced space of configurations. However, in the context of SAWs, one is generally interested not in the set of *all* paths that can be drawn on G , but specifically in the subset of such paths which are rooted at a fixed site. By selecting $p = 1$ in Algorithm 1 however, the location of the second defect becomes fixed and the $p \rightarrow 1, n \rightarrow 0$ limit of Algorithm 1 defines a valid Monte Carlo procedure for simulating the set of all rooted SAWs on G , with fugacity x for the number of steps. In fact, this algorithm is nothing other than (a slight variation of) the Berretti-Sokal algorithm [40] for the grand-canonical (i.e. variable-length) ensemble of SAWs. For the simulations reported in Section 4 therefore, when $n = 0$ we used Algorithm 1 with $p = 1$.

An important practical matter when implementing Algorithm 1 is the need, when $n \neq 0, 1$, to perform a non-local query to determine if the cyclomatic number changes when an update is performed. Consider a spanning subgraph $(V, A) \subseteq G$. Since the number of components, $k(A)$, is related to the cyclomatic number by $k(A) = |V| - |A| + c(A)$, the task of determining whether an edge-update changes the cyclomatic number is equivalent to determining whether it changes the number of connected components. The latter question can be answered by known dynamic connectivity-checking algorithms [41], which take polylogarithmic amortized time. A much simpler approach, which runs in polynomial time, but with a (known) small exponent is simultaneous breadth-first search [42]. We used the latter approach when implementing Algorithm 1 in the simulations presented in Section 4. In practice however it is worth noting that connectivity queries are not actually required at each step, as we now discuss.

To illustrate, we will consider $n > 1$, and suppose the proposed update is to delete an edge uu' which is currently occupied. In this case the acceptance probability equals either $1/(1+x)$ or $1/(1+nx)$, depending on whether or not uu' is a bridge, and we have the bound $1/(1+nx) < 1/(1+x)$ for all $x > 0$. In deciding whether or not to accept the proposed update, we draw a random number r uniformly from $[0, 1]$. If $r < 1/(1+nx)$ then the proposal will be accepted, regardless of whether uu' is a bridge. Likewise, if $r > 1/(1+x)$ then the update will always be rejected. It is therefore only when $1/(1+nx) < r < 1/(1+x)$ that we need to perform connectivity queries to determine whether or not uu' is a bridge, and therefore whether or not

to accept the proposal. A similar observation holds for the proposed addition of an edge, and analogous observations apply also for $n < 1$. Finally, we note also that similar arguments can be used if the acceptance probabilities are chosen using the acceptance function $\min(1, z)$, however the results are rather more cumbersome in that case. This was our primary motivation for using the heat-bath version.

Remark 2.1. It is possible to augment Algorithm 1 with the following additional move: when the two defects collide, move them both to a new vertex of G , chosen uniformly at random. It was found in [32] for the $n = 1$ case that the addition of this extra move does not alter the dynamic universality class of the algorithm, but does slightly improve its efficiency, with the efficiency gain tending to zero as the system size tends to infinity. For the simulations reported in Section 4 we applied this extra move when $n > 0$.

2.2. Coloring algorithm

We now describe an alternative to Algorithm 1 which avoids altogether the need to perform connectivity queries when $n \geq 1$. Consider a finite graph $G = (V, E)$. The key observation is that simulating the $n > 1$ loop model on G is equivalent to simulating the $n = 1$ loop model on appropriately chosen random subgraphs of G . To see this, let us begin with the loop model partition function (4) and introduce auxiliary vertex colorings as follows:

$$Z = \sum_{A \in C(G)} \prod_{C \in \{\text{cycles of } A\}} x^{|C|} \sum_{\sigma_C \in \{r, b\}} [\delta_{\sigma_C, r} + (n-1)\delta_{\sigma_C, b}], \quad (6)$$

$$= \sum_{A \in C(G)} \sum_{\sigma \in \{r, b\}^V} \prod_{ij \in A} \delta_{\sigma_i, \sigma_j} \prod_{C \in \{\text{cycles of } A\}} x^{|C|} [\delta_{\sigma_C, r} + (n-1)\delta_{\sigma_C, b}] \prod_{v \in \{\text{isolated vertices of } A\}} \delta_{\sigma_v, r}. \quad (7)$$

Each vertex can take one of two colors, r(ed) or b(lue), and the leftmost product in (7) implies that each cycle has all of its vertices colored the same color. This fact allows us to unambiguously use the notation σ_C for the color of a cycle C . The expression (7) defines a joint model of loops and vertex colorings, and one can simulate the loop model (4) by simulating the joint model (7). This is similar in spirit to the idea behind the Swendsen-Wang cluster algorithm [43]. Given a loop configuration $A \in C(G)$, the joint model (7) implies that we can obtain a random vertex coloring by coloring all isolated vertices red, and independently coloring each cycle red with probability $1/n$ or blue with probability $(n-1)/n$. This coloring defines two random induced subgraphs of G , one red and one blue, and (7) implies that on the red subgraph the weight of each loop configuration is independent of n , and is in fact just the weight given by the $n = 1$ loop model. Therefore, the loop configuration on the red subgraph can be updated using an $n = 1$ worm algorithm. The weights of loop configurations on the blue subgraph do depend on n , but provided we re-choose the random vertex colorings every so often, to ensure ergodicity, we are free to simply leave the loop configurations on the blue subgraph fixed, since “do-nothing” transitions trivially preserve stationarity with respect to any measure. We therefore consider the red vertices as being *active* and the blue vertices *inactive*. These observations lead to the following algorithm for simulating the $n > 1$ loop model (4).

Algorithm 2 (Colored worm algorithm).

```

loop
  Current state is  $A \in C(G)$ 
  randomly with probability  $p_{\text{color}}$  do
    Color each isolated vertex red

```


Independently color each loop: red with probability $1/n$, and blue otherwise
Identify the induced subgraph of red vertices $G_{\text{red}} = G[V_{\text{red}}]$
end randomized block
Choose, uniformly at random, $v \in V(G_{\text{red}})$
Use $n = 1$ worm updates on G_{red} to make a transition $(A_{\text{red}}, v, v) \rightarrow (A'_{\text{red}}, v', v')$
New state is $A' = A'_{\text{red}} \cup A_{\text{blue}}$
end loop

The above arguments leading to Algorithm 2 can be expressed in a more formal setting using transition matrices, and a formal proof of validity can be given; see [27]. The underlying idea behind this *coloring method* is in fact very general [26]. A similar method was used in [44] to construct a cluster algorithm for the random-cluster model for arbitrary real $q > 1$. Related ideas were also discussed in [45], in the context of a loop model with integer n . We also note that similar ideas were used in an exact mapping between an $O(n)$ and an $O(n - 1)$ model [46].

The probability p_{color} in Algorithm 2 can be set to any desired value in $(0, 1]$. We found empirically that in order to avoid a situation in which almost all of the computer-time is spent on re-coloring, rather than on worm updates, it is advantageous to choose p_{color} to be strictly less than 1. For each given value of $n > 1$ we therefore ran preliminary simulations to tune p_{color} to a value which resulted in roughly equal time being spent of worm updates and color updates.

2.3. Consistency checks

We performed several tests to verify the correctness of the worm algorithms. First, we verified that Algorithms 1 and 2 produced the same results for a number of static observables, including the bond density. Furthermore, we checked the consistency of the results of the worm algorithms for general n with an alternative local algorithm which used plaquette updates. Some care is needed for these tests because, without special provisions, the plaquette algorithm is subject to conservation laws restricting the numbers of nontrivial loops spanning the periodic system. We also performed tests with cluster algorithms for the spin model (2), for the special cases $n = 1$ and $n = 2$. For the latter case, the tests are restricted to the physical range $x \leq 1/2$, which just excludes the critical point, but still allows accurate tests.

3. Observables

In this section we define the observables that we sampled in our simulations, discuss some quantities of interest defined from these observables, and highlight some of their relevant properties. The numerical results of our simulations and finite-size scaling fits for these quantities are then presented in Section 4.

The following observables were sampled in our simulations. All observables were sampled only when the defects coincided, with the exception of the return time, \mathcal{T} , which is defined on the full worm chain. The quantity L denotes the linear system size.

- The number of bonds $\mathcal{N}_b(A) = |A|$.
- The number of loops $\mathcal{N}_l(A) = c(A)$.
- The length of the largest loop \mathcal{L}_1 .

- The mean-square loop length

$$\mathcal{L}_2 := L^{-d} \sum_l |l|^2 \quad (8)$$

where the sum is over all loops l .

- The indicator \mathcal{W}_x for the event that there exists a loop with positive winding number in the x direction. We also sampled \mathcal{W}_y and \mathcal{W}_z , which are defined analogously.
- The time \mathcal{T} between consecutive visits to the Eulerian subspace of $\mathcal{S}(G)$ during a realization of the worm chain.

From these observables we estimated the following quantities:

- The expectations $\langle \mathcal{L}_1 \rangle$ and $\langle \mathcal{L}_2 \rangle$.
- The dimensionless ratio

$$Q_l = \frac{\langle \mathcal{L}_1 \rangle^2}{\langle \mathcal{L}_1^2 \rangle}. \quad (9)$$

The quantity Q_l was used to locate the critical point x_c and estimate the thermal exponent y_l when $n > 0$. It was not studied for $n = 0$ since the configurations are single paths rather than multiple loops in this case.

- The dimensionless ratio

$$Q_b = \frac{\langle \mathcal{N}_b \rangle^2}{\langle \mathcal{N}_b^2 \rangle}. \quad (10)$$

The quantity Q_b was used to locate the critical point x_c and estimate the thermal exponent y_l when $n = 0$. It was not studied for $n > 0$ since $\langle \mathcal{N}_b^k \rangle$ is trivially of order L^{kd} for all x in that case.

- The wrapping probability

$$R := \frac{1}{3} \langle \mathcal{W}_x + \mathcal{W}_y + \mathcal{W}_z \rangle \quad (11)$$

By symmetry, $R = \langle \mathcal{W}_x \rangle = \langle \mathcal{W}_y \rangle = \langle \mathcal{W}_z \rangle$, so the wrapping probability is simply the probability of there existing a loop which has a positive winding number along a fixed coordinate axis. Analogous quantities were shown in [47] to provide a highly effective method for estimating the critical probability of square-lattice site percolation, and various probabilities of this kind can be calculated exactly for the random-cluster model on a square-lattice with toroidal boundary conditions [48, 49]. A notable feature of the wrapping probabilities studied in [47] was their weak finite-size corrections, and the results presented in Section 4 show that such behavior also holds for the loop model on the hydrogen-peroxide lattice.

- The expected time of return $\langle \mathcal{T} \rangle$ to the Eulerian subspace.

It can be shown for integer $n > 0$ that $\langle \mathcal{T} \rangle$ coincides with the susceptibility χ of the n -vector model (2), while for $n = 0$ it coincides with the susceptibility of the self-avoiding walk problem; see Section 3.1 for details. The numerical results presented in [27] for the honeycomb lattice strongly suggest that in fact $\langle \mathcal{T} \rangle \sim \chi$ holds near criticality for arbitrary

real $n > 0$ ², regardless of whether one uses Algorithm 1 or Algorithm 2. Furthermore, the results presented in Section 4 suggest that $\langle \mathcal{T} \rangle \sim \chi$ also holds on the hydrogen peroxide lattice for real non-negative n .

We note that the quantities relating to loop properties, R , $\langle \mathcal{L}_1 \rangle$, $\langle \mathcal{L}_2 \rangle$ and Q_l , were studied for $n > 0$ only.

3.1. Worm return times and susceptibility

In this section we provide a derivation of the result $\chi = \langle \mathcal{T} \rangle$ for integer $n \geq 0$. We consider first the case $n > 0$.

Let $G = (V, E)$ be a finite graph. The two-point correlation function of the model (2) is

$$\langle \mathbf{s}_u \cdot \mathbf{s}_v \rangle = \frac{1}{Z} \text{Tr} \prod_{ij \in E} (1 + n x \mathbf{s}_i \cdot \mathbf{s}_j) \mathbf{s}_u \cdot \mathbf{s}_v \quad (12)$$

where the $\mathbf{s}_i = (s_i^1, \dots, s_i^n) \in \mathbb{R}^n$ are unit vectors and Tr denotes the product over vertices $i \in V$ of normalized integration with respect to some given *a priori* $\langle \cdot \rangle_0$ measure on \mathbb{R}^n . We will focus on three common cases for the spin *a priori* measure, corresponding to the $O(n)$, corner-cubic and face-cubic models. In each case, the *a priori* measure corresponds to uniform measure on a certain compact subset of \mathbb{R}^n . In the case of the $O(n)$ model the spins are constrained to lie on the unit sphere; in the case of the corner-cubic model the spins point to the 2^n corners of the unit hypercube; while in the face-cubic model the spins point to the midpoints of the $2n$ faces of the unit hypercube. We note that all three models coincide with the Ising model when $n = 1$. Furthermore, when $n = 2$ the corner-cubic and face-cubic models coincide, since in this case they are simply related by a rotation of $\pi/4$.

To identify [7] the spin partition function (2) with the loop partition function (4), one begins by expanding out the product over edges in (2), associating a bond of color $\alpha \in \{1, 2, \dots, n\}$ to each edge ij for which the term $n x s_i^\alpha s_j^\alpha$ is selected. One can then attempt to explicitly sum over the spins. It is a common feature of each of the above *a priori* measures that the moments $\langle (s_i^1)^{m_1} (s_i^2)^{m_2} \dots (s_i^n)^{m_n} \rangle_0$ vanish unless each m_α is even. Therefore, only terms for which each vertex is adjacent to an even number of edges of each color can make a non-zero contribution after performing the spin sums. One therefore arrives at a model of edge-disjoint colored loop coverings of G . For graphs of maximum degree 3, one can then simply sum over all ways of coloring the loops to obtain (4).

The same general procedure can be applied to compute a graphical expansion of (12). In this case, the set of bond configurations leading to non-zero contributions is $\mathcal{S}_{u,v}(G)$, the set of all bond configurations with precisely two odd vertices, u and v , introduced in Section 2.1. The summation over bond colorings of the component containing u, v (the *defect cluster*) must be treated somewhat carefully however, and it turns out that the precise result depends on the specific choice of a *a priori measure*. In particular, different *a priori* measures can give different weights depending on the topology of the defect cluster. For graphs of maximum degree 3, the topology of the defect cluster is rather constrained and can be only one of the following: cycle, path, tadpole, dumbbell or theta graph. See Fig. 2. In general, whenever the defect cluster

²The case $n = 0$ was not studied in [27].

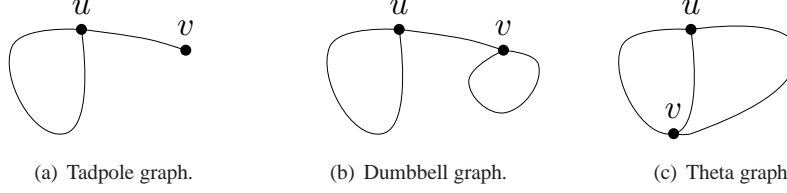


Figure 2: Possible topologies for the defect cluster. Paths and cycles are also possible, but not shown.

is a theta graph it receives an additional model-dependent weight, in addition to $x^{|A|} n^{c(A)}$. A precise statement of the final result is given in the following lemma, whose detailed proof is straightforward and therefore omitted.

Lemma 3.1. *For any graph of maximum degree 3 we have*

$$Z \langle \mathbf{s}_u \cdot \mathbf{s}_v \rangle = \sum_{A \in \mathcal{S}_{u,v}} x^{|A|} n^{c(A)} \Theta(A)$$

where the function $\Theta : \mathcal{S}_{u,v} \rightarrow \mathbb{R}$ is

$$\Theta(A) := \begin{cases} \theta(A), & \text{if the component containing } u \text{ and } v \text{ is a theta graph,} \\ 1, & \text{otherwise,} \end{cases}$$

and

$$\theta(A) := \begin{cases} 1, & \text{face-cubic,} \\ (3n-2)/n^2, & \text{corner-cubic,} \\ 3/(n+2), & O(n). \end{cases}$$

We note that, unlike the corner-cubic and $O(n)$ cases, the result for the face-cubic model does not actually involve special weights for the defect cluster, because distinct colors correspond to orthogonal spin states in this case. Also, we note that, as expected, the expansion for the corner-cubic model coincides with that for the face-cubic model when $n = 1, 2$. The $O(n)$ model only coincides with the face-cubic model for $n = 1$.

Now, from Lemma 3.1 we immediately obtain an expansion for the magnetization. By definition $\mathcal{M} = \sum_{i \in V} \mathbf{s}_i$, so Lemma 3.1 implies

$$\langle \mathcal{M}^2 \rangle = \sum_{u,v \in V} \langle \mathbf{s}_u \cdot \mathbf{s}_v \rangle, \tag{13}$$

$$= \frac{1}{Z} \sum_{(A,u,v) \in \mathcal{S}(G)} x^{|A|} n^{c(A)} \Theta(A), \tag{14}$$

where $\mathcal{S}(G)$ is the state space of the worm dynamics, as defined in Section 2.1, and Z is the partition function of the loop model (4). It should therefore come as no surprise that $\langle \mathcal{M}^2 \rangle$ can be easily sampled via worm dynamics.

Indeed, suppose we construct a worm algorithm on $\mathcal{S}(G)$ for which we chose the acceptance probabilities so as to give detailed balance with an arbitrary probability measure

$$\mathbb{P}_\psi(A, u, v) \propto \psi(A), \quad (A, u, v) \in \mathcal{S}(G). \tag{15}$$

If $\langle \cdot \rangle_\psi$ denotes expectation with respect to $\mathbb{P}_\psi(\cdot)$, then it is obvious that

$$\langle \mathbf{1}_{C(G)} \rangle_\psi = |V| \frac{Z_{C(G)}(\psi)}{Z_{S(G)}(\psi)}, \quad (16)$$

where $Z_{C(G)}(\psi)$ denotes the sum of $\psi(\cdot)$ over $C(G)$, $Z_{S(G)}(\psi)$ the sum of $\psi(\cdot)$ over $S(G)$, and $\mathbf{1}_{C(G)}(\cdot)$ denotes the indicator for the event that $(A, u, v) \in S(G)$ satisfies $A \in C(G)$, or equivalently that $u = v$. Choosing $\psi(A) = x^{|A|} n^{c(A)} \Theta(A)$, and combining (14) and (16) while noting that states in $C(G)$ do not contain theta graphs, it follows that

$$\langle \mathbf{1}_{C(G)} \rangle = \frac{|V|}{\langle \mathcal{M}^2 \rangle} \quad (17)$$

where the expectation on the right is with respect to the n -vector spin measure defined by (2) for a given choice of *a priori* measure, and the expectation on the left is with respect to the corresponding graphical measure on the worm state space, as inferred from Lemma 3.1. The susceptibility of translation invariant systems³ is therefore equal to

$$\chi = \frac{\langle \mathcal{M}^2 \rangle}{|V|} = \frac{1}{\langle \mathbf{1}_{C(G)} \rangle}. \quad (18)$$

In fact, the expression (18) also holds as a relationship between the $n \rightarrow 0, p \rightarrow 1$ limit of Algorithm 1, and the susceptibility of the self-avoiding walk problem. Indeed, taking this limit of Algorithm 1 implies

$$\langle \mathbf{1}_{C(G)} \rangle = \frac{1}{\sum_{A \in \{\text{rooted SAWs on } G\}} x^{|A|}}. \quad (19)$$

The denominator on the right-hand side of (19) is nothing other than the generating function of variable-length rooted SAWs on G , counted according to step length, which is precisely the definition of susceptibility for the SAW problem [50]. We note that in the $n \rightarrow 0, p \rightarrow 1$ limit of Algorithm 1 the quantity $\mathbf{1}_{C(G)}$ is simply the indicator for the 0-step walk.

Finally, since $\langle \mathbf{1}_{C(G)} \rangle$ is the stationary probability of the worm chain occupying a state in $C(G)$, the expected time between consecutive visits to $C(G)$ is simply $\langle \mathcal{T} \rangle = 1/\langle \mathbf{1}_{C(G)} \rangle$, and so for integer $n \geq 0$ we have

$$\langle \mathcal{T} \rangle = \chi. \quad (20)$$

Remark 3.1. For the sake of computational efficiency, the simulations presented in Section 4 used Algorithm 2 when $n > 1$. Algorithm 1 and Algorithm 2 have precisely the same stationary distribution on the subspace $C(G)$, and therefore the estimates they produce for all loop observables defined on $C(G)$ must be the same. However, they do give slightly different weights to the non-Eulerian states in $S(G)$, which implies that $\langle \mathcal{T} \rangle$ will not be precisely equal to the χ in this case. Nonetheless we expect that the scaling behavior of $\langle \mathcal{T} \rangle$ should still be governed by the magnetic exponent y_h . The results for the honeycomb lattice presented in [27] as well as our results for the hydrogen peroxide lattice presented in Section 4 are consistent with this expectation. In order to test this expectation more systematically, we note that one can in principle construct a generalization of Algorithm 2 in which one introduces the vertex colorings to the full worm space $S(G)$ rather than just the subspace $C(G)$. This would provide an interesting generalization of the coloring method presented in [26]. We shall investigate such methods elsewhere.

³I.e. systems on regular lattices with periodic boundary conditions.

4. Simulations

We simulated the loop model (4) on finite hydrogen-peroxide lattices with periodic boundary conditions, for loop fugacities $n = 0, 0.5, 1, 1.5, 2, 3, 4, 5$ and 10 . For $n = 0, 0.5, 1$ we used Algorithm 1, with p set to 1 for $n = 0$ and to $1/2$ for $n = 0.5, 1$. For $n > 1$ we used Algorithm 2, so as to avoid the need for non-local connectivity queries.

For each value of n , we ran simulations of several $L \times L \times L$ systems at several values of x . The length unit is chosen as one half of the 8-site hydrogen-peroxide cell, so that the systems contain L^3 sites. The lattice sizes L were taken in the range 8 to 128. Additional simulations for $L = 256$ were performed at the critical point x_c as estimated from the smaller system sizes. For each choice of (n, x, L) we performed multiple independent simulations, as a means of implementing (trivial) parallelization. For each independent simulation, statistical errors were estimated by partitioning the data into 1000 bins, and computing error bars using blocking. The resulting means and error bars of the independent runs were then combined to produce the final estimates for each choice of (n, x, L) . For $n \neq 0$, we performed between 100 and 300 independent simulations for each choice of (n, x, L) , each simulation consisting of 10^6 returns to the Eulerian subspace, the first 10^4 returns being discarded as burn-in. For $n = 0$, we performed 50 independent simulations for each choice of (x, L) , each simulation consisting of between $0.5 \times 10^6 L^3$ and $1.25 \times 10^6 L^3$ iterations (hits), with the first $10^3 L$ iterations being discarded as burn-in. For the $n = 0$ case we sampled observables every $L^3/4$ iterations, since we found in all cases that taking lags of this size guaranteed the autocorrelation function for \mathcal{N}_b was smaller than 0.1. (See Section 4.5 for relevant definitions concerning autocorrelations.)

For each of the quantities discussed in Section 3 we performed a least-squares fit of our Monte Carlo data to an appropriate finite-size scaling (FSS) expression. As a precaution against excessive corrections to scaling, we imposed a lower cutoff $L \geq L_{\min}$ on the data points admitted to the fit, and we studied systematically the effects on the fit due to variations of the value of L_{\min} . The error bars that we report for our fits are composed of the statistical error (one standard error) plus a subjective estimate of the systematic error. To estimate the systematic error we compared multiple distinct fits for each quantity, corresponding to different choices of correction terms included in the FSS formulas, and/or different choices of L_{\min} . Given that the FSS formulas are nonlinear, we used the Levenberg-Marquardt algorithm to perform the least-squares fits.

4.1. The wrapping probability R

According to finite-size scaling theory, the expected behavior of the dimensionless wrapping probability $R(x, L)$ as a function of the linear system size L and temperature-like parameter x is

$$R = R^{(0)} + a_1(x - x_c)L^{y_t} + a_2(x - x_c)^2L^{2y_t} + a_3(x - x_c)^3L^{3y_t} + a_4(x - x_c)^4L^{4y_t} + c(x - x_c)^2L^{y_t} + b_1L^{y_1} + b_2L^{y_2} + b_3L^{y_3} + e(x - x_c)L^{y_t+y_1} + \dots \quad (21)$$

where x_c denotes the critical point, y_t the thermal exponent, and y_1, y_2, y_3 are negative correction-to-scaling exponents.

We fitted Eq. (21) to our Monte Carlo data, and the resulting estimates for x_c and y_t are reported in Table 2. In each fit the values of the correction-to-scaling exponents were fixed, while x_c, y_t were free parameters. For $n = 1$, the correction-to-scaling exponents were fixed to $y_1 = -0.815, y_2 = -1.963$, and $y_3 = -3.375$ [51], while for all other $n > 0$ we set $y_1 = -0.85, y_2 = -1.8$ and $y_3 = -3$. The values of y_1 and y_2 are based on estimates found in [52] for $n = 0, 1, 2, 3$ and the supposedly weak dependence of these exponents on n .

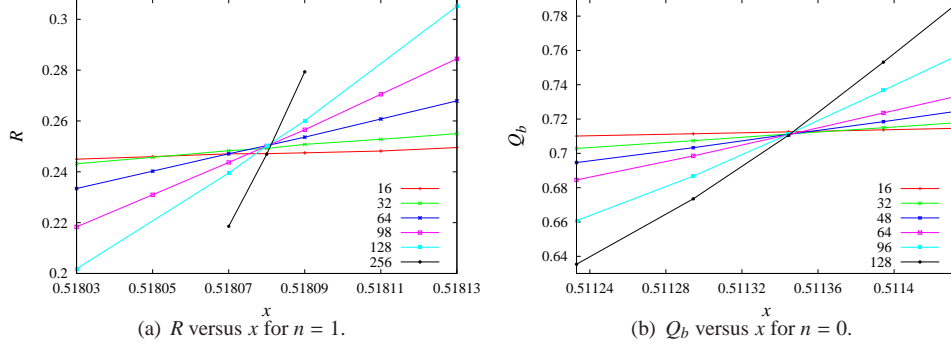


Figure 3: Wrapping probability R for the $n = 1$ loop model and dimensionless ratio Q_b for self-avoiding walks ($n = 0$), versus the bond (step-length) fugacity x , for linear system sizes 16 to 256.

Table 2: Estimated critical point x_c and thermal exponent y_t for a number of values of the loop fugacity n , as determined from least-squares fits of the wrapping probability R .

n	x_c	y_t	$R^{(0)}$	a_1	b_1
0.5	0.5146078(6)	1.651(5)	0.1467(2)	1.02(3)	-0.08(3)
1	0.5180815(3)	1.588(2)	0.2524(3)	1.41(1)	-0.031(5)
1.5	0.5217878(5)	1.539(4)	0.3326(5)	1.47(3)	-0.062(5)
2	0.5257533(5)	1.489(3)	0.3990(4)	1.48(1)	-0.077(6)
3	0.5345904(8)	1.398(3)	0.5020(6)	1.33(1)	-0.144(5)
4	0.544904(2)	1.329(8)	0.5861(6)	1.08(2)	-0.18(2)
5	0.557096(5)	1.275(12)	0.6548(6)	0.82(3)	-0.21(2)
10	0.67367(2)	1.142(15)	0.8638(5)	0.12(2)	-0.23(2)

For $n \leq 3$, each of the coefficients a_1, \dots, a_4, b_1, c were free parameters in the fits, while the coefficient e was set identically to zero. As a means of gauging systematic errors, we performed fits with b_2, b_3 set identically to zero, as well as fits in which b_2, b_3 were free parameters, and compared the resulting estimates for y_t and x_c . For each $n \leq 3$, our final estimates of y_t and x_c and their error bars were obtained by comparing these two fits. For $n = 4, 5, 10$, the strength of the corrections to scaling demanded that we include all terms in (21) in our fits, so that each of the coefficients $a_1, \dots, a_4, b_1, \dots, b_3, c, e$ were free parameters in these fits.

4.2. The dimensionless ratios Q_l and Q_b

As a consistency check on the values of x_c and y_t determined from R , we performed analogous fits of Q_l , again on the basis of (21), with the same procedure for fixing the correction exponents and coefficient values. The resulting estimates for x_c and y_t are reported in Table 3. The agreement with the corresponding estimates produced by the R fits is clearly excellent.

The results for R and Q_l applied only to $n > 0$, however analogous fits can be performed for $n = 0$ using Q_b . Following the same procedure as for R and Q_l we thereby obtained the estimated values of x_c and y_t for $n = 0$ presented in Table 3. While this treatment of the SAW case appears natural within the context of the general loop model, we note that it may be considered somewhat unusual to deliberately study SAWs on a finite system. Indeed, one reason why SAWs are often considered easier to study via simulation than other models in statistical mechanics is precisely because it is possible to study SAWs on an infinite lattice. One might therefore be led to expect

Table 3: Estimated critical point x_c and thermal exponent y_t for a number of values of the loop fugacity n , as determined from least-squares fits of the dimensionless ratios Q_l and Q_b .

n	x_c	y_t	$Q^{(0)}$	a_1	b_1
0	0.5113445(2)	1.701(2)	0.7017(2)	0.675(4)	0.11(2)
0.5	0.5146084(7)	1.653(5)	0.4858(6)	0.578(6)	0.012(6)
1	0.5180813(4)	1.586(7)	0.6158(4)	0.836(5)	0.042(5)
1.5	0.5217884(7)	1.532(8)	0.6884(5)	0.750(6)	0.052(5)
2	0.5257539(7)	1.487(3)	0.7316(4)	0.644(6)	0.066(4)
3	0.534595(4)	1.398(4)	0.7827(3)	0.435(5)	0.073(3)
4	0.544907(4)	1.332(7)	0.8086(4)	0.270(6)	0.080(7)
5	0.557108(8)	1.280(10)	0.8252(4)	0.162(5)	0.12(2)
10	0.67373(7)	1.145(30)	0.8573(3)	0.016(5)	0.10(2)

Table 4: Estimated values of the scaling exponents y_l and y_h , for a number of values of the loop fugacity n , as determined from least-squares fits of $\langle \mathcal{L}_2 \rangle$ and $\langle \mathcal{T} \rangle$. For $n \leq 1$, Algorithm 1 was used, while Algorithm 2 was used for $n > 1$.

n	Fits for $\langle \mathcal{L}_2 \rangle$		Fits for $\langle \mathcal{T} \rangle$		
	y_l	a_0	y_h	a_0	a_1
0	—	—	2.4875(7)	0.796(5)	-6.257(2)
0.5	1.723(3)	0.64(2)	2.482(4)	1.11(2)	6.8(1)
1	1.734(4)	1.16(3)	2.483(3)	0.97(2)	5.04(6)
1.5	1.755(3)	1.44(3)	2.482(3)	0.91(2)	3.80(5)
2	1.765(3)	1.80(2)	2.483(2)	0.86(2)	3.16(3)
3	1.795(3)	2.18(2)	2.482(2)	0.80(2)	2.32(4)
4	1.816(3)	2.62(2)	2.483(2)	0.77(2)	1.63(4)
5	1.834(6)	2.9(1)	2.483(3)	0.74(2)	1.22(4)
10	1.901(8)	5.6(2)	2.486(3)	0.75(4)	0.26(5)

that Q_b will be a rather poor estimator for the critical point. However, it is clear from Fig. 3(b) that this is not the case, and in fact the sharpness of the point of intersection of the Q_b curves in Fig. 3(b) is quite remarkable. It would be interesting to see if such behavior holds on other lattices, such as the simple-cubic lattice.

4.3. Mean-square loop length

The finite-size scaling behavior of $\langle \mathcal{L}_2 \rangle$ is expected to be [27]

$$\langle \mathcal{L}_2 \rangle = L^{2y_l-d}(a_0 + a_1(x - x_c)L^{y_t} + b_1L^{y_1} + b_2L^{y_2} + b_3L^{y_3} + \dots) \quad (22)$$

where y_l is the fractal dimension characterizing loop length. We fitted Eq. (22) to our Monte Carlo data for $\langle \mathcal{L}_2 \rangle$, fixing y_t and x_c to their values as reported in Table 2. The corrections-to-scaling exponents were fixed according to the procedure described for R . And again, as a means of gauging systematic errors, for $n \leq 3$ we performed fits with b_2, b_3 set identically to zero, as well as fits in which b_2, b_3 were free parameters, and compared the resulting estimates for y_l and x_c . The resulting estimates for y_l are reported in Table 4.

4.4. Susceptibility χ - average worm return time

The finite-size scaling behavior of $\langle \mathcal{T} \rangle$ is expected to be [27]

$$\langle \mathcal{T} \rangle = L^{2y_h-d}(a_0 + a_1(x - x_c)L^{y_t} + b_1L^{y_1} + \dots) \quad (23)$$

where y_h is the magnetic exponent. We fitted Eq. (23) to our Monte Carlo data for $\langle \mathcal{T} \rangle$, fixing y_t and x_c to their values as reported in Table 2 (Table 3 for $n = 0$). For the fits to (23) it was found sufficient to include only one correction-to-scaling term, and y_1 was fixed using the same procedure as for the R fits. The resulting estimates for y_h are reported in Table 4.

A remark concerning our use of Algorithm (2) is in order. For $n \leq 1$, the values of $\langle \mathcal{T} \rangle$ were computed using Algorithm 1, and so the discussion of Section 3.1 implies that for $n = 0, 1$ the mean return time $\langle \mathcal{T} \rangle$ is precisely equal to the susceptibility of the SAW and Ising models respectively. For $n > 1$ however, we used Algorithm 2 in our simulations, and so the discussion in Section 3.1 does not imply the exact equality of $\langle \mathcal{T} \rangle$ and χ in these cases. However, it was found empirically in [27] that on the honeycomb lattice while $\langle \mathcal{T} \rangle$ may not be precisely equal to χ when using Algorithm 2, the two quantities scale in the same way at criticality, so measuring $\langle \mathcal{T} \rangle$ in Algorithm 2 was indeed found to be an accurate method for computing y_h . As we discuss further in Section 5, our estimates for y_h on the hydrogen peroxide lattice also agree within error bars with previously-obtained results for the $O(n)$ universality class.

4.5. Dynamic behavior

When $n = 1$, Algorithms 1 and 2 coincide, and in this case a careful study of the dynamic critical behavior was carried out in [32]. In particular, it was found that in three dimensions the Li-Sokal bound (see below) appeared to be sharp. In order to explore the efficiency of the worm algorithms for more general n , we studied the dynamic critical behavior of both Algorithm 1 and Algorithm 2 for the case $n = 2$. For comparison, we also studied the dynamic critical behavior of a local plaquette update algorithm.

Consider an observable O . A realization of the worm Markov chain gives rise to a time series $O(t)$. The autocorrelation function of O is defined to be [39]

$$\rho_O(t) = \frac{\langle O(0)O(t) \rangle - \langle O \rangle^2}{\text{var}(O)},$$

where $\langle \cdot \rangle$ denotes expectation with respect to the stationary distribution. From $\rho_O(t)$ we define the integrated autocorrelation time as

$$\tau_{\text{int},O} \equiv \frac{1}{2} \sum_{t=-\infty}^{\infty} \rho_O(t), \quad (24)$$

and the exponential autocorrelation time as

$$\tau_{\text{exp},O} \equiv \limsup_{t \rightarrow \pm\infty} \frac{|t|}{-\log |\rho_O(t)|}. \quad (25)$$

Finally, the exponential autocorrelation time of the system is defined as

$$\tau_{\text{exp}} = \sup_O \tau_{\text{exp},O} \quad (26)$$

where the supremum is taken over all observables O . This autocorrelation time therefore samples the relaxation rate of the slowest mode of the system. All observables that are not orthogonal to this slowest mode satisfy $\tau_{\text{exp},O} = \tau_{\text{exp}}$.

The autocorrelation times typically diverge as a critical point is approached, most often like $\tau \sim \xi^z$, where ξ is the spatial correlation length and z is a dynamic exponent. This phenomenon

is referred to as critical slowing-down [39]. In the case of a finite lattice at criticality, we define the dynamic critical exponents $z_{\text{int},O}$, $z_{\text{exp},O}$ and z_{exp} by

$$\tau_{\text{int},O} \sim L^{z_{\text{int},O}}, \quad \tau_{\text{exp},O} \sim L^{z_{\text{exp},O}}, \quad \tau_{\text{exp}} \sim L^{z_{\text{exp}}}. \quad (27)$$

Note that when defining z_{exp} and $z_{\text{int},O}$ it is natural to express time in units of *sweeps* of the lattice, i.e. L^d hits. However, when using Algorithms 1 or 2, observables are sampled only when the chain visits the Eulerian subspace. Given that $\langle \mathcal{T} \rangle$ scales like the susceptibility, this occurs roughly every L^{d-2X_h} iterations, where X_h is the magnetic scaling dimension. Since one sweep therefore takes of order L^{2X_h} visits to $C(G)$, in units of “visits to $C(G)$ ” we have $\tau \sim L^{z+2X_h}$. Consequently, we fit our dynamic data to the ansatz

$$\tau_{\text{int},O} = a + bL^{z_{\text{int},O}+2X_h} \quad (28)$$

to obtain the exponent $z_{\text{int},O}$.

In this work, we determined $\rho_O(t)$ and $\tau_{\text{int},O}$ for the observables \mathcal{N}_b , \mathcal{L}_2 , and \mathcal{N}_l . This was done for $n = 2$, using both Algorithm 1 and Algorithm 2. We find that the slowest of these observable is \mathcal{N}_b . Figure 4 shows $\rho_{\mathcal{N}_b}$ as a function of $t/\tau_{\text{int},\mathcal{N}_b}$, where a nearly pure exponential decay is observed, suggesting $z_{\text{exp}} \approx z_{\text{int},\mathcal{N}_b}$.

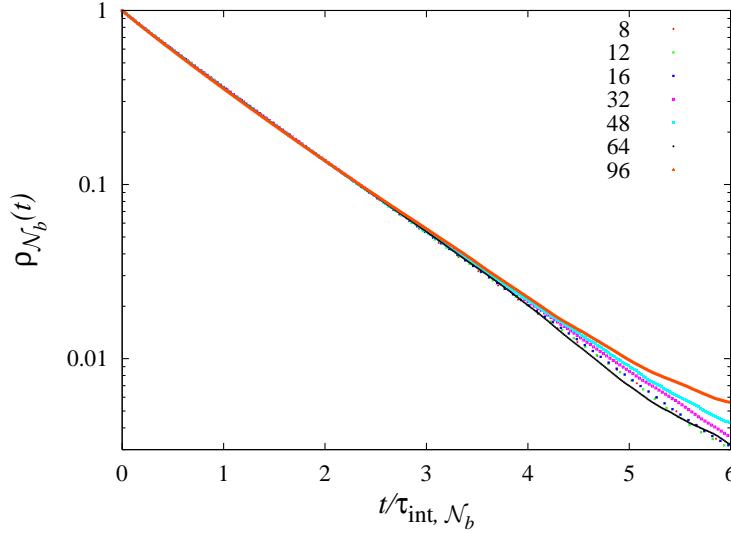


Figure 4: Autocorrelation function $\rho_{\mathcal{N}_b}(t)$ versus $t/\tau_{\text{int},\mathcal{N}_b}$. The almost-pure exponential decay of $\rho_{\mathcal{N}_b}(t)$ suggests $z_{\text{exp}} \approx z_{\text{int},\mathcal{N}_b}$.

For Algorithm 1 we find $z_{\text{int},\mathcal{N}_b} = 0.19$ (3), while for Algorithm 2 we find $z_{\text{int},\mathcal{N}_b} = 0.243$ (12). It is perhaps unsurprising that the bonds should decorrelate faster when using Algorithm 1 compared with Algorithm 2, since in the latter case a non-trivial subset of the bonds is always being held fixed at any given time. We emphasize, however, that these values of $z_{\text{int},\mathcal{N}_b}$ are inherent properties of the underlying Markov chains, and do not encode any information regarding the amount of CPU time required in practice to execute each MC update. In particular, despite the fact that Algorithm 1 suffers from slightly weaker critical slowing down, in practice Algorithm 2 actually outperforms our implementation of Algorithm 1, because it avoids the need for costly non-local connectivity queries.

For comparison, we also determined $z_{\text{int}, \mathcal{N}_b}$ for a simple plaquette-update algorithm. Like worm algorithms, these plaquette update algorithms can be used for arbitrary real $n > 0$. However, a rough estimation for $n = 2$ yields $z_{\text{int}, \mathcal{N}_b} = 2.26$ (5), which is significantly larger than for the worm algorithm. Similar values of z for plaquette algorithms have been observed previously [35]. In addition, we note that the performance of the worm algorithm compares very favorably with Wolff’s embedding algorithm [25], which is perhaps the most widely-used Monte Carlo method for studying $O(n)$ spin models, and which was found in [53] to have $z_{\text{int}, \text{energy}} = 0.46(3)$ when $(n, d) = (2, 3)$.

Finally, it is interesting to compare these results with the $n = 1$ case [32] where it was found that $z_{\text{int}, \mathcal{N}_b} \approx \alpha/\nu \approx 0.17$. This implies that the Li-Sokal bound [33] $z_{\text{int}, \mathcal{N}_b} \geq \alpha/\nu$, which can be easily generalized to worm algorithms, appears to be sharp for $n = 1$. By contrast, for $n = 2$ we have $\alpha/\nu \approx -0.026$, so that the Li-Sokal bound does not appear to be close to sharp in this case.

5. Discussion

Using the worm algorithms introduced in [27], we have studied the critical behavior of the loop model (4) on a three-dimensional 3-regular lattice, the hydrogen peroxide lattice, for a range of integer and non-integer loop fugacities $0 \leq n \leq 10$. To our knowledge, this is the first direct Monte Carlo study of loop models with general n in three dimensions. A study of the dynamic critical behavior of these algorithms for $n = 2$ shows that the critical-slowness is only very weak; not only is it much weaker than for local plaquette-update algorithms, but also significantly weaker than for the Wolff embedding algorithm [25, 53]. Combined with the previous study of the $n = 1$ case [32], these results strongly suggest that worm algorithms provide a very effective method for studying loop models in three dimensions.

Our simulations show that the loop model (1) undergoes a continuous phase transition, with critical exponents that depend on the loop fugacity n . Our best estimates of the exponents y_t and y_h are reported in Table 5. For integer n , these exponent estimates are consistent with the $O(n)$ universality class; for comparison, we list in Table 5 a number of relevant exponent estimates from the literature. For the cases $n = 0$ and $n = 1$ this is entirely to be expected, since exact mappings unambiguously identify the loop model with the SAW and Ising models respectively, and these mappings are valid in a range of x which includes the critical point x_c . In fact, for the $n = 0$ case Algorithm 1 actually directly simulates the grand canonical ensemble of SAWs. More generally, one might expect from the identity (2) that the loop model should in fact be in the same universality class as the n -vector model for any integer n . However, for $n > 1$ the situation is slightly more subtle, for two reasons. Firstly, the spin model to which the loop model maps has positive weights only for $x < 1/n$, and for $n \geq 2$ we find empirically that x_c lies outside this range. Secondly, and perhaps more importantly, the mapping from the spin model (2) to the loop model (1) is many-valued; it maps the loop model (1) to a number of distinct spin models, whose Hamiltonians possess different symmetry groups and which therefore might be expected to belong to distinct universality classes.

To put these observations in context, let us briefly recount the relationship between the $O(n)$ model and the two discrete cubic models discussed in Section 3.1. Renormalization group arguments [24] predict the following scenario. There exists a critical n_c , believed to be ≈ 3 in three dimensions, below which the cubic models and $O(n)$ models share the same universality class, but beyond which they do not. For $n > n_c$, the face-cubic model is believed to undergo a first order transition, while the critical behavior of the corner-cubic model is believed to be governed by a distinct *cubic* fixed point. The discrepancies between the predicted exponent values of the $O(n)$

Table 5: Comparison of the estimated loop-model exponents y_l and y_h with existing literature. For $n = 0$ we compare with known SAW exponents, while for integer $n \geq 1$ we compare with the corresponding exponents of the $O(n)$ spin model. No error bounds were given in [54] for their estimate of y_l at $n = 10$.

n	y_l		y_h	
	This work	Literature	This work	Literature
0	1.701(2)	1.7018(6)[55], 1.70179(5)[56], 1.70185(2)[57]	2.4875(7)	2.4849(5)[58]
0.5	1.653(5)	—	2.482(4)	—
1	1.588(2)	1.5868(3)[51]	2.483(3)	2.48180(8)[59], 2.4816(1)[51]
1.5	1.538(4)	—	2.482(3)	—
2	1.488(3)	1.4888(2)[60]	2.483(2)	2.4810(1)[60]
3	1.398(2)	1.406(10)[61], 1.405(2)[62]	2.482(2)	2.4830(5)[61], 2.4811(15)[62]
4	1.332(7)	1.3375(15)[63], 1.333(4)[62]	2.483(2)	2.4820(2)[63], 2.4820(15)[62]
5	1.275(12)	1.309(7)[64]	2.483(3)	2.4845(15)[64]
10	1.142(15)	1.164(—)[54]	2.486(3)	2.488(1)[54]

and cubic fixed points at $n = 3$ are too small to detect using current approximations, however they increase with n . Indeed, as $n \rightarrow \infty$, the $O(n)$ model approaches the spherical model [11, 1], with exponents $y_{l,\text{spherical}} = 1$ and $y_{h,\text{spherical}} = 5/2$, while the corner-cubic model can be reinterpreted as a constrained Ising model [65] so that its exponents are given by a Fisher renormalization of the Ising exponents, $y_{l,\text{cubic}} = d - y_{l,\text{Ising}} = 1.4132(3)$ and, $y_{h,\text{cubic}} = y_{h,\text{Ising}} = 2.4816(1)$. For finite n these exponents have corrections of $O(1/n)$; for example [66] predicts $y_{l,\text{cubic}} = 1.416(12)$, $1.401(16)$, $1.404(12)$ for $n = 3, 4, 8$.

Our estimates of y_l reported in Table 5 agree within error bars with the corresponding $O(n)$ values from the literature when $n \leq 4$. For $n = 5, 10$ the agreement is not perfect, but still quite convincing. Furthermore, the n -dependence of our y_l estimates is entirely consistent with the limiting $O(n)$ value of $y_l = 1$ as $n \rightarrow \infty$. The behavior of y_h in Table 5, while only weakly dependent on n , is also consistent with the $O(n)$ universality class. By contrast, our y_l estimates are entirely inconsistent with the cubic fixed point. Based on these observations it seems reasonable to conclude that the critical behavior of the loop model (1) on the hydrogen peroxide lattice belongs to the $O(n)$ universality class.

Finally, we note that the literature also contains results for the loop exponent y_l in three dimensions. Recently, Winter et al. [35] determined the fractal dimension of the high-temperature graphs at criticality for the Ising and the XY model on a cubic lattice. Using a plaquette update algorithm, they estimated the fractal dimensions of the Ising and the XY model as $D = 1.7349(65)$ and $D = 1.7626(66)$ respectively. Furthermore, Prokof'ev and Svistunov [67] reported the fractal dimension of the graph expansion of the complex $|\phi|^4$ theory at its critical point as $D = 1.7655(20)$. From the expected equivalence in universality we may compare this results with our result of y_l for the $n = 2$ model. As can be seen from the Table 4, our estimates of y_l are in good agreement with the cited literature.

Acknowledgments

This work was supported in part by the National Nature Science Foundation of China under Grant No. 10975127, the Specialized Research Fund for the Doctoral Program of Higher Education under Grant No. 20113402110040, and the Chinese Academy of Sciences. It was also supported under the Australian Research Council's Discovery Projects funding scheme (project number DP110101141), and T.G. is the recipient of an Australian Research Council Future Fel-

lowship (project number FT100100494). H.B. thanks the Lorentz Fund for financial support, and the University of Science and Technology of China in Hefei for hospitality extended to him.

References

- [1] H. E. Stanley, Dependence of critical properties on dimensionality of spins, *Phys. Rev. Lett.* 20 (1968) 589–592.
- [2] R. B. Potts, Some generalized order-disorder transformations, *Proc. Cambridge Philos. Soc.* 48 (1952) 106–109.
- [3] F. Y. Wu, The Potts model, *Rev. Mod. Phys.* 54 (1982) 235–268.
- [4] F. Y. Wu, Potts model of magnetism, *J. Appl. Phys.* 55 (1984) 2421–2425.
- [5] C. M. Fortuin and P. W. Kasteleyn, Random-cluster model 1: Introduction and relation to other models, *Physica* 57 (1972) 536–564.
- [6] G. R. Grimmett, *The Random-Cluster Model*, Springer, New York, 2006.
- [7] E. Domany, D. Mukamel, B. Neinhuis and A. Schwimmer, Duality relations and equivalences for models with $O(n)$ and cubic symmetry, *Nucl. Phys. B* 190 (1981) 279–287.
- [8] P. Di Francesco, P. Mathieu and D. Sénéchal, *Conformal Field Theory*, Springer-Verlag, New York, 1997.
- [9] W. Kager and B. Nienhuis, A Guide to Stochastic Löwner Evolution and Its Applications, *J. Stat. Phys.* 115 (2004) 1149–1229.
- [10] J. Cardy, SLE for theoretical physicists, *Ann. Phys.* 318 (2005) 81–118.
- [11] T. H. Berlin and M. Kac, The Spherical Model of a Ferromagnet, *Phys. Rev.* 86 (1952) 821–835.
- [12] P.-G. de Gennes, *Scaling Concepts in Polymer Physics*, Cornell University Press, Ithaca, NY, 1979.
- [13] B. Nienhuis, Exact Critical Point and Critical Exponents of $O(n)$ Models in Two Dimensions, *Phys. Rev. Lett.* 49 (1982) 1062–1065.
- [14] B. Nienhuis, Critical behavior of two-dimensional spin models and charge asymmetry in the Coulomb gas, *J. Stat. Phys.* 34 (1984) 731–761.
- [15] R. J. Baxter, q colourings of the triangular lattice, *J. Phys. A: Math. Gen.* 19 (1986) 2821–2839.
- [16] R. J. Baxter, Chromatic polynomials of large triangular lattices, *J. Phys. A: Math. Gen.* 20 (1987) 5241–5261.
- [17] E. Brézin, J. C. Le Guillou and J. Zinn-Justin, Field Theoretical Approach to Critical Phenomena, in: C. Domb and M. S. Green (Ed.), *Phase Transitions and Critical Phenomena*, Vol. 6, Academic Press, New York, 1976, pp. 125–247.
- [18] K. G. Wilson, Feynman-graph expansion for critical exponents, *Phys. Rev. Lett.* 28 (1972) 548–551.
- [19] R. Abe, Expansion of a critical exponent in inverse powers of spin dimensionality, *Progr. Theor. Phys.* 48 (1972) 1414–1415.
- [20] S. -K. Ma, Critical Exponents for Charged and Neutral Bose Gases above λ Points, *Phys. Rev. Lett.* 29 (1972) 1311–1314.
- [21] M. Suzuki, Critical exponents and scaling relations for the classical vector model with long-range interactions, *Phys. Lett. A* 42 (1972) 5–6.
- [22] R. A. Ferrell and D. J. Scalapino, Order-Parameter Correlations within the Screening Approximation, *Phys. Rev. Lett.* 29 (1972) 413–416.
- [23] D. P. Landau and K. Binder, *A guide to Monte Carlo simulations in statistical physics*, 3rd Edition, Cambridge University Press, Cambridge, 2009.
- [24] A. Pelissetto and E. Vicari, Critical phenomena and renormalization-group theory, *Phys. Rep.* 368 (2002) 549–727.
- [25] U. Wolff, Collective Monte Carlo Updating for Spin Systems, *Phys. Rev. Lett.* 62 (1989) 361–364.
- [26] Youjin Deng, Timothy M. Garoni, Wenan Guo, Henk W. J. Blöte and Alan D. Sokal, Cluster Simulations of Loop Models on Two-Dimensional Lattices, *Phys. Rev. Lett.* 98 (2007) 120601.
- [27] Q. Liu, Y. Deng and T. M. Garoni, Worm Monte Carlo study of the honeycomb-lattice loop model, *Nucl. Phys. B* 846 (2011) 283–315.
- [28] A. F. Wells, *Three-Dimensional Nets and Polyhedra*, John Wiley & Sons Inc., New York, 1977.
- [29] J. A. Leu, D. D. Betts and C. J. Elliott, High-temperature critical properties of the Ising model on a triple of related lattices, *Canadian Journal of Physics* 47 (1969) 1671–1689.
- [30] J. A. Leu, Self-avoiding walks on a pair of three dimensional lattices, *Physics Letters A* 29 (1969) 641–642.
- [31] N. Prokof’ev and B. Svistunov, Worm Algorithms for Classical Statistical Models, *Phys. Rev. Lett.* 87 (2001) 160601.
- [32] Youjin Deng, Timothy M. Garoni and Alan D. Sokal, Dynamic Critical Behavior of the Worm Algorithm for the Ising Model, *Phys. Rev. Lett.* 99 (2007) 110601.
- [33] X.-J. Li and A. D. Sokal, Rigorous Lower Bound on the Dynamic Critical Exponents of the Swendsen-Wang Algorithm, *Phys. Rev. Lett.* 63 (1989) 827–830.
- [34] G. Ossola, A. D. Sokal, Dynamic critical behavior of the Swendsen-Wang algorithm for the three-dimensional Ising model, *Nucl. Phys. B* 691 (2004) 259–291.

- [35] F. Winter, W. Janke, and A. M. J. Schakel, Geometric properties of the three-dimensional Ising and XY models, *Phys. Rev. E* 77 (2008) 061108.
- [36] U. Wolff, Simulating the all-order strong coupling expansion III: $O(N)$ sigma/loop models, *Nucl. Phys. B* 824 (2010) 254–272.
- [37] U. Wolff, Erratum to “Simulating the all-order strong coupling expansion III: $O(N)$ sigma/loop models” [*Nucl. Phys. B* 824 (2010) 254], *Nucl. Phys. B* 834 (2010) 395–397.
- [38] N. Metropolis, A. Rosenbluth, M. Rosenbluth, A. Teller and E. Teller, Equation of State Calculations by Fast Computing Machines, *J. Chem. Phys.* 21 (1953) 1087–1092.
- [39] A. D. Sokal, Monte Carlo methods in Statistical Mechanics: Foundations and new algorithms, in: C. DeWitt-Morette, P. Cartier, A. Folacci (Eds.), *Functional Integration: Basics and Applications*, Plenum, New York, 1997, pp. 131–192.
- [40] A. Berretti and A. D. Sokal, New Monte Carlo Method for the Self-Avoiding Walk, *J. Stat. Phys.* 40 (1985) 483–531.
- [41] J. Holm, K. de Lichtenberg and M. Thorup, Poly-Logarithmic Deterministic Fully-Dynamic Algorithms for Connectivity, Minimum Spanning Tree, 2-Edge, and Biconnectivity, *J. ACM* 48 (2001) 723–760.
- [42] Youjin Deng, Wei Zhang, Timothy M. Garoni, Alan D. Sokal and Andrea Sportiello, Some geometric critical exponents for percolation and the random-cluster model, *Phys. Rev. E* 81 (2010) 020102(R).
- [43] R. H. Swendsen and Jian-Sheng Wang, Nonuniversal critical dynamics in Monte Carlo simulations, *Phys. Rev. Lett.* 58 (1987) 86–88.
- [44] L. Chayes and J. Machta, Graphical representations and cluster algorithms II, *Physica A.* 254 (1998) 477–516.
- [45] U. Wolff, Simulating the all-order strong coupling expansion IV: $CP(N-1)$ as a loop model, *Nucl. Phys. B* 832 (2010) 520–537.
- [46] H. W. J. Blöte and B. Nienhuis, Critical behaviour and conformal anomaly of the $O(n)$ model on the square lattice, *J. Phys. A* 22 (1989) 1415–1438.
- [47] M. E. J. Newman, R. M. Ziff, Efficient monte carlo algorithm and high-precision results for percolation, *Phys. Rev. Lett.* 85 (2000) 4104–4107.
- [48] H. T. Pinson, Critical percolation on the torus, *J. Stat. Phys.* 75 (1994) 1167–1177.
- [49] L. P. Arguin, Homology of fortuin-kasteleyn clusters of potts models on the torus, *J. Stat. Phys.* 109 (2002) 301–310.
- [50] N. Madras and G. Slade, *The Self-Avoiding Walk*, Birkhäuser, Boston, 1996.
- [51] Y. Deng and H. W. J. Blöte, Simultaneous analysis of several models in the three-dimensional Ising universality class, *Phys. Rev. E* 68 (2003) 036125.
- [52] K. E. Newman and E. K. Riedel, Critical exponents by the scaling-field method: The isotropic N -vector model in 3 dimensions, *Phys. Rev. B* 30 (1984) 6615–6638.
- [53] M. Hasenbusch and S. Meyer, Critical exponents of the 3D XY model from cluster update Monte Carlo, *Phys. Lett. B* 241 (1990) 238–242.
- [54] S. A. Antonenko and A. I. Sokolov, Critical exponents for a three-dimensional $O(n)$ -symmetric model with $n > 3$, *Phys. Rev. E* 51 (1995) 1894–1898.
- [55] A. Pelissetto and E. Vicari, Renormalized four-point coupling constant in the three-dimensional $O(N)$ model with $N \rightarrow 0$, *J. Phys. A* 40 (2007) F539–F550.
- [56] H.-P. Hsu, W. Nadler and P. Grassberger, Scaling of Star Polymers with 1-80 Arms, *Macromolecules* 37 (2004) 4658–4663.
- [57] N. Clisby, Accurate Estimate of the Critical Exponent ν for Self-Avoiding Walks via a Fast Implementation of the Pivot Algorithm, *Phys. Rev. Lett.* 104 (2010) 055702.
- [58] S. Caracciolo, M. S. Causo, and A. Pelissetto, High-precision determination of the critical exponent γ for self-avoiding walks, *Phys. Rev. E* 57 (1998) R1215–R1218.
- [59] M. Campostrini, A. Pelissetto, P. Rossi, and E. Vicari, 25th-order high-temperature expansion results for three-dimensional Ising-like systems on the simple-cubic lattice, *Phys. Rev. E* 65 (2002) 066127.
- [60] M. Campostrini, M. Hasenbusch, A. Pelissetto, and E. Vicari, Theoretical estimates of the critical exponents of the superfluid transition in ^4He by lattice methods, *Phys. Rev. B* 74 (2006) 144506.
- [61] M. Campostrini, M. Hasenbusch, A. Pelissetto, P. Rossi, and E. Vicari, Critical exponents and equation of state of the three-dimensional Heisenberg universality class, *Phys. Rev. B* 65 (2002) 144520.
- [62] M. Hasenbusch, E. Vicari, Anisotropic perturbations in three-dimensional $O(N)$ -symmetric vector models, *arXiv:1108.0491v1*.
- [63] Y. Deng, Bulk and surface phase transitions in the three-dimensional $O(4)$ spin model, *Phys. Rev. E* 73 (2006) 056116.
- [64] A. Butti and F. Parisen Toldin, The critical equation of state of the three-dimensional $O(N)$ universality class: $N > 4$, *Nucl. Phys. B* 704 (2005) 527–551.
- [65] A. Aharony, Dependence of Universal Critical Behaviour on Symmetry and Range of Interaction, in: C. Domb

- and M. S. Green (Ed.), Phase Transitions and Critical Phenomena, Vol. 6, Academic Press, New York, 1976, pp. 357–424.
- [66] J. M. Carmona, A. Pelissetto and E. Vicari, N-component Ginzburg-Landau Hamiltonian with cubic anisotropy: A six-loop study, *Phys. Rev. B* 61 (2000) 15136–15151.
- [67] N. Prokof'ev and B. Svistunov, Comment on “Hausdorff Dimension of Critical Fluctuations in Abelian Gauge Theories”, *Phys. Rev. Lett.* 96 (2006) 219701.